PCCP

PAPER

View Article Online
View Journal | View Issue

Cite this: *Phys. Chem. Chem. Phys.*, 2018, **20**, 29236

Phonon mode contributions to thermal conductivity of pristine and defective β-Ga_2O_3†

Zhequan Yan and Satish Kumar*

Received 12th August 2018,
Accepted 31st October 2018

DOI: 10.1039/c8cp05139a

rsc.li/pccp

β-Ga_2O_3 is emerging as a promising semiconductor for high-power high-frequency electronics. The low thermal conductivity of pristine β-Ga_2O_3 and the presence of defects, which can further suppress the thermal conductivity, will result in critical challenges for the performance and reliability of β-Ga_2O_3-based devices. We use first-principles density functional theory (DFT) along with the Boltzmann transport equation (BTE) to predict the phonon transport properties of pristine and defective β-Ga_2O_3. Our predictions of anisotropic thermal conductivity are in good agreement with the experimental results. We find that the low-frequency optical phonon modes make a significant contribution to the thermal conductivity compared to the acoustic modes, especially in the [010] direction because of the non-negligible group velocities of the low-frequency optical branches. To better understand the influence of defects on the phonon transport mechanism, we investigate the thermal conductivity of β-Ga_2O_3 with 1–2% oxygen or gallium vacancies considering the defect-induced phonon scatterings. We observe that the Ga vacancies lead to a larger suppression in the thermal conductivity than in those with O vacancies. Furthermore, we find that the vacancies have more influence on the optical modes than on acoustic modes, which suppress the contribution of optical modes to the thermal conductivity. The results from this work will help us understand the mechanism of phonon transport considering the influence of defects and provide insights for the future design of β-Ga_2O_3-based electronic devices.

I. Introduction

Because of the large bandgap and the resultant large electrical breakdown strength, β-Ga_2O_3 emerged as a promising semiconductor which can sustain large voltages, making it attractive for high-power devices.[1] In contrast to the band gap of ~3.4 eV of GaN,[2,3] the β-Ga_2O_3 exhibits a larger bandgap of ~4.8 eV.[4] The larger breakdown voltage and the larger breakdown field (~8 MV cm^{-1})[5] than GaN make the Baliga's figure of merit (FOM) of β-Ga_2O_3 (3200) four times larger than that of GaN (860).[3] The unique electronic/optical properties and the lower cost of manufacturing of bulk crystals of β-Ga_2O_3 than those of GaN and SiC make it a promising candidate for high-power high-frequency devices, such as solar blind UV photodetectors,[6] power rectifiers,[7] gas sensors,[1,8] as well as power MOSFETs and MESFETs.[9–11]

High power dissipation in β-Ga_2O_3 devices can cause critical challenges, *e.g.*, it can significantly affect the performance and reliability of these devices.[12] The relatively low thermal conductivity of β-Ga_2O_3 (one-tenth of GaN[13,14]) can lead to excess self-heating that must be mitigated in order to utilize β-Ga_2O_3 in high-frequency devices.[15] Various thermal management approaches need to be investigated for the β-Ga_2O_3 devices, similar to but probably more innovative compared to what has been done with the GaN power devices to enable effective heat removal during high power operation.[16–18] Therefore, it is necessary to understand the thermal transport in β-Ga_2O_3 to better control the hot spot temperature in its active devices and for the design of packaging and thermal solutions. A few studies have focused on the prediction and the measurement of the thermal conductivity of β-Ga_2O_3. A recent computational study reported a thermal conductivity of 16.06 W mK^{-1}, 21.54 W mK^{-1}, and 21.15 W mK^{-1} in the directions of [100], [010], and [001], respectively, at room temperature by solving the linearized Boltzmann transport equation.[19] However, these results were not in great agreement with the experimental results.[20–22] And the mechanism of the phonon transport in β-Ga_2O_3 is not well understood yet.

Due to the imperfection of growth processes, point vacancies[23,24] may exist in β-Ga_2O_3 which can provide promising opportunities for tailoring its electrical properties such as the band structure,[25] conductivity,[24,26–28] and optical properties[29] such as the luminescence spectrum[30] for various device applications. However, the point defects like oxygen and gallium vacancies could suppress the thermal transport, reduce thermal conductivity and make

G. W. Woodruff School of Mechanical Engineering, Georgia Institute of Technology, Atlanta, GA, USA. E-mail: satish.kumar@me.gatech.edu

† Electronic supplementary information (ESI) available. See DOI: 10.1039/c8cp05139a

the thermal management even more challenging.[31,32] No study has focused on exploring the effect of point vacancies on the thermal transport in bulk β-Ga_2O_3. The understanding of how oxygen and gallium vacancies suppress the thermal transport in bulk β-Ga_2O_3 is far from being completed.

In this study, we use first-principles density functional theory (DFT) along with the Boltzmann transport equations (BTE) to predict the phonon transport properties of pristine and defective β-Ga_2O_3. The thermal conductivities of bulk β-Ga_2O_3 along three crystal directions are calculated based on the iterative solution of the BTE. Our predictions of thermal conductivity using the conventional unit cell are in good agreement with the experimental results.[20–22] To better understand the influence of defects on the phonon transport mechanism, we further investigate the thermal conductivity with 1–2% oxygen and gallium vacancies, respectively. The model for estimating the effect of point vacancies on phonon properties is developed by considering contributions of the defect-induced phonon scattering, which is caused by the missing mass of the oxygen or gallium atoms. The Phonon modes' contribution to the thermal conductivity is studied along with the influence of the point vacancies. We find that in the pristine β-Ga_2O_3, optical phonon modes make a significant contribution to the thermal conductivity compared to the acoustic modes. Furthermore, the point vacancies have more influence on the optical modes than on acoustic modes, which suppress the contribution of optical modes to the thermal conductivity.

II. Models and computational methods

β-Ga_2O_3 is a monoclinic crystal with the space group $C2/m$ containing 20 atoms per conventional unit cell. Although recent work[33] reported that the ambiguity in defining the Brillouin zone for transferring the conventional monoclinic unit cell to a reduced primitive cell has been resolved, we still use the 20-atom conventional unit cell (Fig. 1) instead of the 10-atom unit cell in order to exclude the potential risk of the Brillouin zone shape variations.[33–35] Considering this, the conventional unit cell will provide the anisotropic thermal conductivity along three crystallographic directions directly.

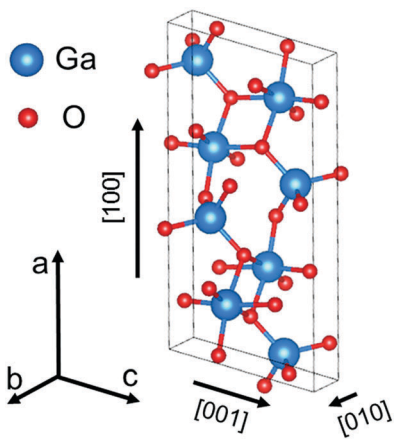

Fig. 1 The conventional unit cell of the bulk β-Ga_2O_3. The blue and red spheres represent gallium atoms and oxygen atoms, respectively.

We perform first-principles DFT simulation to calculate the total energy of the bulk β-Ga_2O_3 using Vienna ab initio simulation package (VASP).[36] A plane-wave basis set and the projector augmented-wave (PAW) method are used with the Perdew–Burke–Ernzerhof (PBE) exchange–correlation functional.[37–39] A 500 eV kinetic energy cutoff is used to perform the structure optimization and calculate the second-order harmonic and third-order anharmonic interatomic force constants (IFCs). The system energy convergence criterion is set to be 10^{-9} eV. The force convergence criterion is set to be -0.001 eV $Å^{-1}$. The unit cell of β-Ga_2O_3 with 20 atoms shown in Fig. 1 is optimized with a $4 \times 16 \times 8$ grid for Brillouin zone sampling. The optimized lattice parameters are a = 12.45 Å, b = 3.08 Å, and c = 5.86 Å with β = 103.76°, which are in good agreement with the computational[19] and experimental results.[40] Using these optimized lattice parameters, the $1 \times 4 \times 2$ supercell of the 20-atom unit cell is assembled for the calculation of IFCs. The second-order harmonic IFCs and third-order anharmonic IFCs are calculated using the finite difference method in the Phonopy package.[41] The displacement length of each atom from its equilibrium position is 0.01 Å. The interactions between atoms up to the 4th nearest neighboring shell are taken into account for the third-order IFC calculation. Using the second-order and third-order IFCs obtained from the first-principles calculations, the phonon relaxation times and the anisotropic thermal conductivities of bulk β-Ga_2O_3 along various directions are calculated using Fermi's Golden rule[42] with the iterative solution of the Boltzmann transport equation.[43,44] For solving the BTE, a $5 \times 17 \times 9$ k-space sampling mesh was used for Brillouin zone sampling over temperatures ranging from 150 K to 500 K. Furthermore, the effects of oxygen or gallium vacancies in the bulk β-Ga_2O_3 on the phonon scattering rate and thermal conductivity are also considered by adding the defect-induced phonon scattering to the anharmonic phonon scattering rate:[32]

$$1/\tau = 1/\tau_{anh} + 1/\tau_V \quad (1)$$

where $1/\tau_{anh}$ is the intrinsic anharmonic phonon scattering rate. $1/\tau_V$ is the defect-induced phonon scattering rate which is caused by the missing of oxygen or gallium atoms in the crystal. It can be expressed as,[45–48]

$$1/\tau_V = x\left(-\frac{M_V}{M} - 2\right)^2 \frac{\pi}{2} \frac{\omega^2 g(\omega)}{G} \quad (2)$$

where x is the density of vacancies, M is the average mass per atom, M_V is the mass of the missing atom, $g(\omega)$ is the phonon density of states (DOSs), and G is the number of atoms in the crystal.

III. Results and discussion

The results indicate that β-Ga_2O_3 has significant anisotropy of the thermal conductivity along the three directions of basis vectors of the conventional unit cell, see Fig. 2. The largest

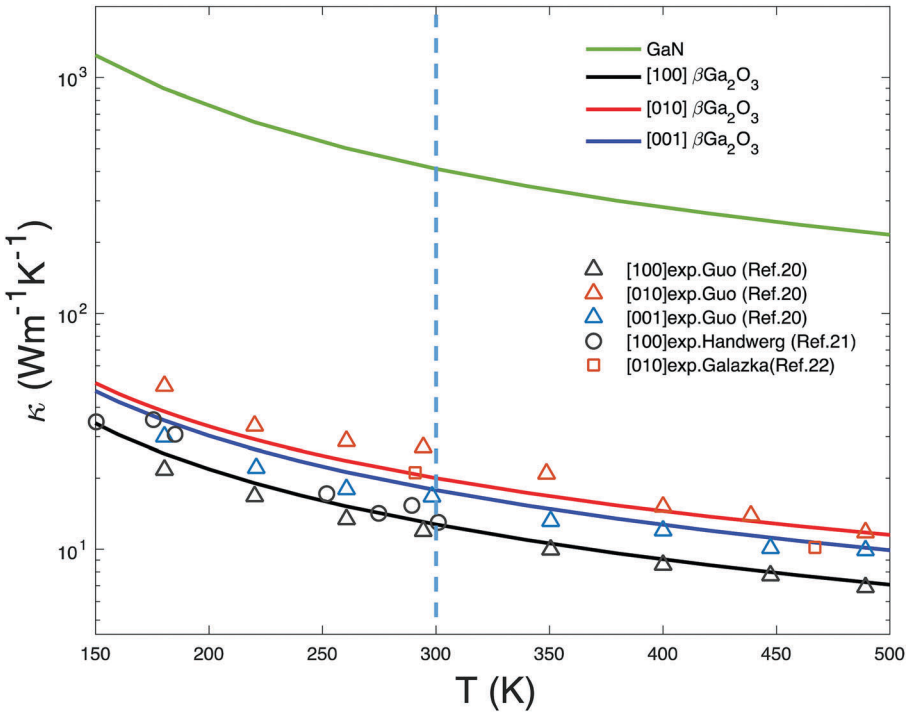

Fig. 2 Temperature-dependent thermal conductivity of the bulk β-Ga_2O_3 and GaN compared to the experimental measurements.

Table 1 Thermal conductivity of the bulk β-Ga_2O_3 at 300 K

Crystallographic orientation	This study	Experiment	Simulation[19]
[100]	12.73	10.9 ± 0.7,[20] 13 ± 1[21]	16.06
[010]	20.00	27.1 ± 2,[20] 21[22]	21.54
[001]	17.80	14.7 ± 1.4[20]	21.15

Table 2 The thermal conductivity of the bulk β-Ga_2O_3 is fitted to a functional form of $\kappa(T) = AT^{-m}$ ($T > 200$ K). The fitting value of each parameter in the equation is listed in the table

Crystallographic orientation	This study		Experiment[20]		Simulation[19]	
	A ($\times 10^4$)	m	A ($\times 10^4$)	m	A ($\times 10^4$)	m
[100]	1.35	1.22	1.06	1.21	1.99	1.13
[010]	2.01	1.21	3.28	1.27	2.47	1.27
[001]	1.78	1.20	0.814	1.12	3.5	1.26

thermal conductivity of β-Ga_2O_3 is observed in the direction of [010] with the value of 20.00 W mK^{-1} at room temperature. Our observation is in good agreement with the experimental results[20–22] and the previous theoretical study,[19] especially in the directions of [100] and [001], as shown in Table 1. We also fit the thermal conductivity of the bulk β-Ga_2O_3 to the functional form of $\kappa(T) = AT^{-m}$ in the range of 150–500 K. The fitting value of each parameter in the equation is listed in Table 2. We compare the temperature dependent thermal conductivity of bulk β-Ga_2O_3 with bulk GaN in the range of 150–300 K. The thermal conductivity of bulk β-Ga_2O_3 is much lower than that of GaN, which can be explained by the phonon lifetime shown in Fig. 3(a). β-Ga_2O_3 has a much shorter phonon lifetime than GaN in the entire frequency domain. This is supported by the three-phonon scattering phase space in Fig. 3(b) which indicates the volume of phase space available for three-phonon scattering. This could be a consequence of a smaller band-gap or absence of a band-gap between the acoustic and optical phonon bands of β-Ga_2O_3 in different crystallographic directions (see Fig. 5(a)). The three-phonon scattering phase space is another way to indicate the likelihood of phonons being scattered. This shows that the phase space of β-Ga_2O_3 is larger than that of GaN, which means GaN has fewer channels for three-phonon scatterings leading to the longer phonon lifetime and larger thermal conductivity.

To better understand the mechanism of phonon transport in β-Ga_2O_3, we calculate the phonon modes' contribution to the thermal conductivity along the three directions, which is shown in Fig. 4. We find that the optical modes (<10 THz) play a critical role in the thermal transport of β-Ga_2O_3, especially in the [010] direction, which is also supported by Fig. S1 (ESI†). However, this observation indicates that the contributions of the low-frequency optical modes to the thermal conductivity are not negligible compared to the acoustic modes, which is a different characteristic compared to some 2-D semiconductors such as graphene and MoS_2.[49,50] To further understand it, we calculate the phonon dispersions along three basis vectors of the conventional unit cell which is shown in Fig. 5(a). One of the explanations for the high contribution of optical modes is that the group velocities of the optical modes cannot be neglected (Fig. 5(a) and Fig. S2, ESI†). The smaller band-gap between the acoustic and optical phonon bands and hence the

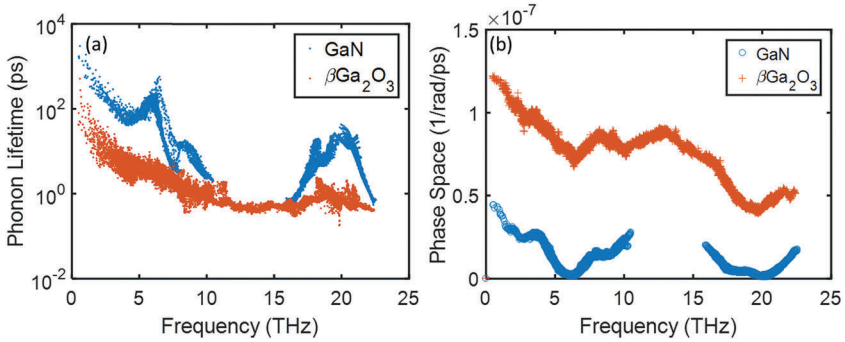

Fig. 3 (a) Angular frequency dependent phonon lifetime of the bulk β-Ga_2O_3 and GaN at 300 K. (b) Three-phonon scattering phase space of the bulk β-Ga_2O_3 and GaN.

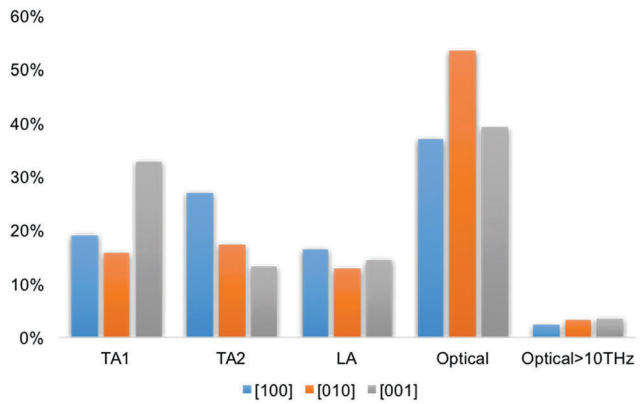

Fig. 4 Phonon mode contribution to the thermal conductivity of pristine bulk β-Ga_2O_3 along three basis vectors of the conventional unit cell at room temperature.

larger three-phonon scattering phase space are also attributed to the lower conductivity. However, this cannot explain the observation of the largest thermal conductivity of β-Ga_2O_3 in the direction of [010] in both simulations and experiments considering the fact that no band-gap is observed along the [010] direction, while gaps exist in the [100] and [001] directions; this was also mentioned by Santia.[19] In Fig. 4, we find the optical modes have 53.45% contribution to the thermal conductivity in [010], which does not have an optical phonon band-gap, but 36.98% and 39.18% in [100] and [001], respectively, which have the gaps. Compared to [010], relatively flat optical phonon branches which have smaller phonon group velocities can be observed in the [100] and [001] directions (shown in Fig. S2, ESI†), which suggests a lower thermal conductivity. A strong contribution of optical modes to thermal conductivity has been found in other semiconducting materials such as GaN,[13] Ca_2N,[51] and graphyne.[52]

In addition, between the transverse acoustic (TA) modes, the TA2 mode has the largest contribution in the [100] and [010] directions. The TA1 mode has the largest contribution in the [001] direction. This can be explained by the flattening of the longitudinal acoustic (LA) modes which may be caused by the hybridization between the low energy optical modes and LA modes. As a result, the lower group velocities of LA phonons result in a lower thermal conductivity. The hybridization is also another reason for the strong optical phonon contributions.

In order to understand how the phonon transport and mode contributions are influenced by the defects, we plot the

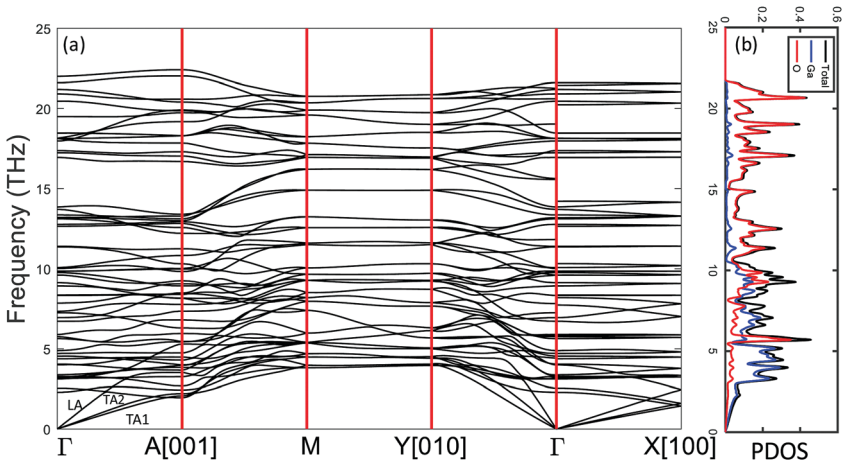

Fig. 5 (a) Phonon dispersions of the bulk β-Ga_2O_3 with the conventional unit cell. (b) Phonon partial density of states (PDOS) of the bulk β-Ga_2O_3, gallium atoms and oxygen atoms.

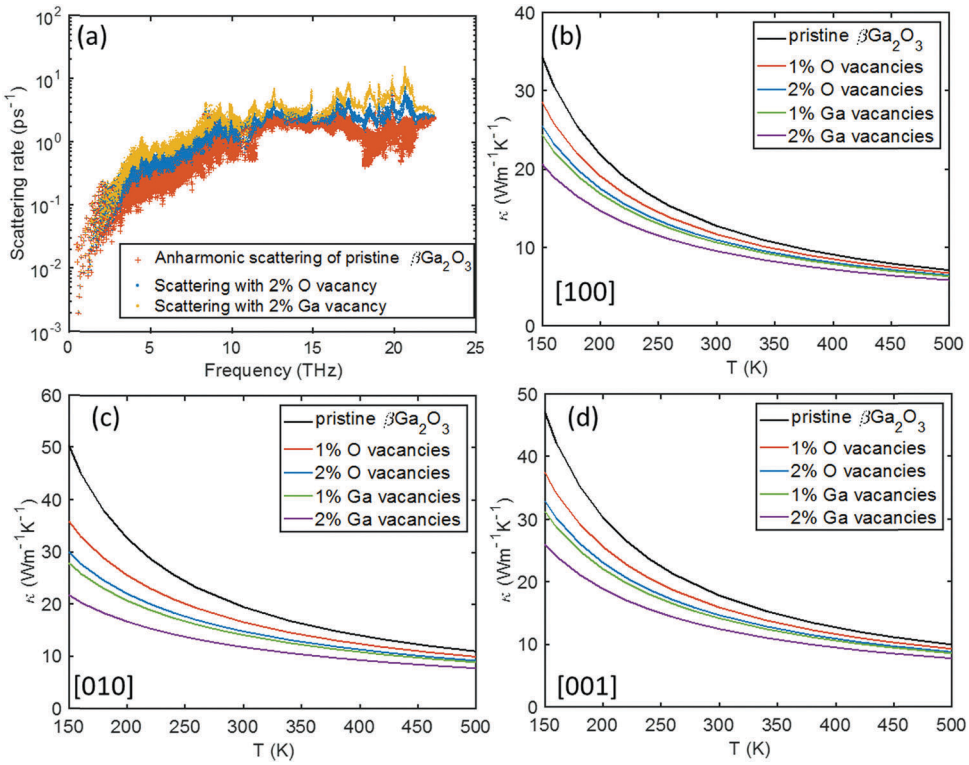

Fig. 6 (a) Angular frequency dependent anharmonic and defect-induced phonon scattering rates of the bulk β-Ga_2O_3 with 2% oxygen vacancies and gallium vacancies at 300 K, respectively. (b–d) Temperature-dependent thermal conductivity of the defective β-Ga_2O_3 with oxygen and gallium vacancies along the directions of (b) [100], (c) [010], and (d) [001].

anharmonic and defect-induced phonon scattering rates of β-Ga_2O_3 in Fig. 6(a), the thermal conductivity of bulk β-Ga_2O_3 with 1–2% oxygen and gallium vacancies along three crystallographic directions in Fig. 6(b–d), and phonon mode contribution to the thermal conductivity under the influence of oxygen vacancies in Fig. 7. The results indicate that at room temperature, 1% and 2% oxygen vacancies decrease the thermal conductivity by 8.5% and 14.3% in the [100] direction, 14.9% and 24.1% in the [010] direction, and 10.7% and 17.4% in the [001] direction, respectively. 1% and 2% Ga vacancies decrease the thermal conductivity by 16.6% and 25.3% in the [100] direction, 27.6% and 39.4% in the [010] direction, and 20.4% and 29.9% in the [001] direction, respectively. A drastic reduction in the thermal conductivity of graphene and CNT due to vacancies has been reported by Fthenakis *et al.*,[53] which is much larger than that of β-Ga_2O_3 for similar vacancy percentages. This can be explained by the fact that under the influence of the defect-induced phonon scattering, the decrease in the phonon mean-free path (MFP) of graphene is much larger than that of β-Ga_2O_3 due to the much larger MFP of pristine graphene. For future convenience in device modeling, the thermal conductivities of the defective bulk β-Ga_2O_3 with the O and Ga vacancies are also fitted to the functional form of $\kappa(T) = AT^{-m}$. The fitting value of A and m in the equation can be found in Table 3. Based on our

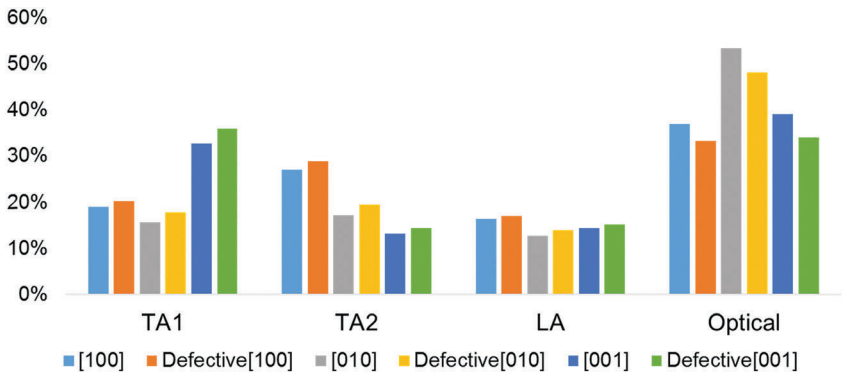

Fig. 7 Phonon mode contribution to the thermal conductivity of defective bulk β-Ga_2O_3 under the influence of 1% oxygen vacancies along three crystallographic orientations at room temperature.

Table 3 The thermal conductivity of the bulk β-Ga_2O_3 under the influence of oxygen vacancies and gallium vacancies is fitted to a functional form of $\kappa(T) = AT^{-m}$ ($T > 200$ K). The fitting value of each parameter in the equation is listed in the table

	O vacancy (1%)		O vacancy (2%)		Ga vacancy (1%)		Ga vacancy (2%)	
Crystallographic orientation	A ($\times 10^3$)	M	A ($\times 10^3$)	m	A ($\times 10^3$)	m	A ($\times 10^3$)	m
[100]	8.92	1.16	6.26	1.11	5.42	1.09	3.32	1.03
[010]	6.27	1.04	3.23	0.96	2.84	0.93	1.43	0.84
[001]	9.94	1.13	6.67	1.07	5.71	1.05	3.44	0.98

defect model (eqn (1) and (2)), the missing atom at a vacancy site results in a mass difference (compared to the average mass of the cell), which results in the kinetic energy and potential energy change. The defect-induced phonon scatterings result in the suppression of the thermal conductivity. Due to the heavier mass of the gallium atom than that of the oxygen atom, the gallium point vacancies could result in a larger kinetic energy and potential energy change than oxygen vacancies, which leads to a larger defect-induced phonon scattering and suppression in the thermal conductivity. Furthermore, the oxygen vacancies have more influence on the optical modes than on the acoustic modes, which leads to a larger suppression in the contribution of optical modes to the thermal conductivity. In other words, under the influence of defects, the percentage of acoustic modes' contribution to the thermal conductivity increases, although the absolute value of thermal conductivity contribution is decreased. To illustrate why the introduced oxygen vacancies suppress the contribution of the optical phonon modes to the thermal conductivity, we investigate the phonon partial density of states (PDOS) of the bulk β-Ga_2O_3, shown in Fig. 5(b). We find that the DOSs of the optical modes are larger than those of acoustic modes. In addition, oxygen atoms in the bulk β-Ga_2O_3 make the highest contribution to the optical energy. Due to the correlation between the phonon DOSs and the defect-induced phonon scattering rate as shown in eqn (2), the defect-induced phonon scatterings for optical modes would have higher impact on the thermal conductivity than that of acoustic modes. The gallium vacancies have similar effects and trends on the mode contributions to the thermal conductivity.

IV. Conclusions

In conclusion, we investigate the thermal conductivity and phonon mode contributions of pristine and defective β-Ga_2O_3 via first-principles calculation and the phonon Boltzmann transport equation. For the pristine β-Ga_2O_3, we report a thermal conductivity of 12.73 W mK^{-1}, 20.00 W mK^{-1}, and 17.80 W mK^{-1} in the direction of [100], [010], and [001], respectively, which are in good agreement with the experimental results. We also find that the optical phonon modes make a significant contribution to the thermal conductivity compared to the acoustic modes, especially in the [010] direction because of the non-negligible group velocities of the low-frequency optical branches and the hybridization between the low energy optical modes and LA modes. For the bulk β-Ga_2O_3 with oxygen vacancies, we find that 1% and 2% oxygen vacancies decrease the thermal conductivity by 8.5% and 14.3% in the [100] direction, 14.9% and 24.1% in the [010] direction, and 10.7% and 17.4% in the [001] direction, respectively, at room temperature. 1% and 2% Ga vacancies decrease the thermal conductivity by 16.6% and 25.3% in the [100] direction, 27.6% and 39.4% in the [010] direction, and 20.4% and 29.9% in the [001] direction, respectively, due to the larger defect-induced phonon scatterings. Furthermore, the vacancies have more influence on the optical modes than on acoustic modes, which leads to a larger suppression of the contribution of optical modes to the thermal conductivity. The results from this work will help us understand the mechanism of phonon transport considering the influence of defects and provide insights for the future design of β-Ga_2O_3-based electronic devices.

Conflicts of interest

There are no conflicts to declare.

References

1 S. Pearton, J. Yang, P. H. Cary IV, F. Ren, J. Kim, M. J. Tadjer and M. A. Mastro, *Appl. Phys. Rev.*, 2018, **5**, 011301.
2 A. Mang and K. Reimann, *Solid State Commun.*, 1995, **94**, 251–254.
3 K. Sasaki, A. Kuramata, T. Masui, E. G. Víllora, K. Shimamura and S. Yamakoshi, *Appl. Phys. Express*, 2012, **5**, 035502.
4 K. Sasaki, M. Higashiwaki, A. Kuramata, T. Masui and S. Yamakoshi, *J. Cryst. Grow.*, 2013, **378**, 591–595.
5 M. Higashiwaki, K. Sasaki, A. Kuramata, T. Masui and S. Yamakoshi, *Appl. Phys. Lett.*, 2012, **100**, 013504.
6 S. Oh, M. A. Mastro, M. J. Tadjer and J. Kim, *ECS J. Solid State Sci. Technol.*, 2017, **6**, Q79–Q83.
7 J. Yang, S. Ahn, F. Ren, S. Pearton, S. Jang and A. Kuramata, *IEEE Electron Device Lett.*, 2017, **38**, 906–909.
8 S. Nakagomi, T. Sai and Y. Kokubun, *Sens. Actuators, B*, 2013, **187**, 413–419.
9 S. Krishnamoorthy, Z. Xia, C. Joishi, Y. Zhang, J. McGlone, J. Johnson, M. Brenner, A. R. Arehart, J. Hwang and S. Lodha, *Appl. Phys. Lett.*, 2017, **111**, 023502.
10 H. Zhou, M. Si, S. Alghamdi, G. Qiu, L. Yang and D. Y. Peide, *IEEE Electron Device Lett.*, 2017, **38**, 103–106.
11 M. J. Tadjer, N. A. Mahadik, V. D. Wheeler, E. R. Glaser, L. Ruppalt, A. D. Koehler, K. D. Hobart, C. R. Eddy and F. J. Kub, *ECS J. Solid State Sci. Technol.*, 2016, **5**, P468–P470.
12 J. Tsao, S. Chowdhury, M. Hollis, D. Jena, N. Johnson, K. Jones, R. Kaplar, S. Rajan, C. Van de Walle and E. Bellotti, *Adv. Electron. Mater.*, 2018, **4**, 1600501.

13 X. Wu, J. Lee, V. Varshney, J. L. Wohlwend, A. K. Roy and T. Luo, *Sci. Rep.*, 2016, **6**, 22504.
14 L. Lindsay, D. Broido and T. Reinecke, *Phys. Rev. Lett.*, 2012, **109**, 095901.
15 M. A. Mastro, A. Kuramata, J. Calkins, J. Kim, F. Ren and S. Pearton, *ECS J. Solid State Sci. Technol.*, 2017, **6**, P356–P359.
16 B. Bayraktaroglu, *Assessment of gallium oxide technology*, Air Force Research Laboratory, Sensors Directorate WPAFB United States, 2017.
17 M. J. Tadjer, T. J. Anderson, K. D. Hobart, T. I. Feygelson, J. D. Caldwell, C. R. Eddy, F. J. Kub, J. E. Butler, B. Pate and J. Melngailis, *IEEE Electron Device Lett.*, 2012, **33**, 23–25.
18 P.-C. Chao, K. Chu, C. Creamer, J. Diaz, T. Yurovchak, M. Shur, R. Kallaher, C. McGray, G. D. Via and J. D. Blevins, *IEEE Trans. Electron Devices*, 2015, **62**, 3658–3664.
19 M. D. Santia, N. Tandon and J. Albrecht, *Appl. Phys. Lett.*, 2015, **107**, 041907.
20 Z. Guo, A. Verma, X. Wu, F. Sun, A. Hickman, T. Masui, A. Kuramata, M. Higashiwaki, D. Jena and T. Luo, *Appl. Phys. Lett.*, 2015, **106**, 111909.
21 M. Handwerg, R. Mitdank, Z. Galazka and S. F. Fischer, *Semicond. Sci. Technol.*, 2015, **30**, 024006.
22 Z. Galazka, K. Irmscher, R. Uecker, R. Bertram, M. Pietsch, A. Kwasniewski, M. Naumann, T. Schulz, R. Schewski and D. Klimm, *J. Cryst. Grow.*, 2014, **404**, 184–191.
23 B. Kananen, L. Halliburton, K. Stevens, G. Foundos and N. Giles, *Appl. Phys. Lett.*, 2017, **110**, 202104.
24 J. Varley, J. Weber, A. Janotti and C. Van de Walle, *Appl. Phys. Lett.*, 2010, **97**, 142106.
25 B. Kananen, L. Halliburton, E. Scherrer, K. Stevens, G. Foundos, K. Chang and N. Giles, *Appl. Phys. Lett.*, 2017, **111**, 072102.
26 L. Dong, R. Jia, B. Xin, B. Peng and Y. Zhang, *Sci. Rep.*, 2017, **7**, 40160.
27 L. Dong, R. Jia, C. Li, B. Xin and Y. Zhang, *J. Alloys Compd.*, 2017, **712**, 379–385.
28 E. Chikoidze, A. Fellous, A. Perez-Tomas, G. Sauthier, T. Tchelidze, C. Ton-That, T. T. Huynh, M. Phillips, S. Russell and M. Jennings, *Mater. Today Phys.*, 2017, **3**, 118–126.
29 X. Ma, Y. Zhang, L. Dong and R. Jia, *Results Phys.*, 2017, **7**, 1582–1589.
30 L. Binet and D. Gourier, *J. Phys. Chem. Solids*, 1998, **59**, 1241–1249.
31 L. Chen, Y. Zhang, X. Wang, B. Jalan, S. Chen and Y. Hou, *J. Phys. Chem. C*, 2018, **122**, 11482–11490.
32 Z. Yan, M. Yoon and S. Kumar, *2D Mater.*, 2018, **5**, 031008.
33 H. Peelaers and C. G. Van de Walle, *Phys. Status Solidi B*, 2015, **252**, 828–832.
34 W. Setyawan, *Comput. Mater. Sci.*, 2010, **49**, 299.
35 M. Mohamed, C. Janowitz, I. Unger, R. Manzke, Z. Galazka, R. Uecker, R. Fornari, J. Weber, J. Varley and C. Van de Walle, *Appl. Phys. Lett.*, 2010, **97**, 211903.
36 G. Kresse and J. Furthmüller, *Phys. Rev. B: Condens. Matter Mater. Phys.*, 1996, **54**, 11169.
37 J. P. Perdew, *Phys. Rev. B: Condens. Matter Mater. Phys.*, 1986, **33**, 8822–8824.
38 G. Kresse and D. Joubert, *Phys. Rev. B: Condens. Matter Mater. Phys.*, 1999, **59**, 1758.
39 J. P. Perdew, K. Burke and M. Ernzerhof, *Phys. Rev. Lett.*, 1996, **77**, 3865.
40 J. Åhman, *Acta Crystallogr., Sect. C: Cryst. Struct. Commun.*, 1996, **52**, 1336.
41 A. Togo and I. Tanaka, *Scr. Mater.*, 2015, **108**, 1–5.
42 A. Maradudin and A. Fein, *Phys. Rev.*, 1962, **128**, 2589.
43 W. Li, J. Carrete, N. A. Katcho and N. Mingo, *Comput. Phys. Commun.*, 2014, **185**, 1747–1758.
44 D. Broido, M. Malorny, G. Birner, N. Mingo and D. Stewart, *Appl. Phys. Lett.*, 2007, **91**, 231922.
45 C. Ratsifaritana and P. Klemens, *Int. J. Thermophys.*, 1987, **8**, 737–750.
46 P. Klemens and D. Pedraza, *Carbon*, 1994, **32**, 735–741.
47 P. Klemens, *Proc. Phys. Soc., London, Sect. A*, 1955, **68**, 1113.
48 G. Xie, Y. Shen, X. Wei, L. Yang, H. Xiao, J. Zhong and G. Zhang, *Sci. Rep.*, 2014, **4**, 5085.
49 Z. Yan, L. Chen, M. Yoon and S. Kumar, *Nanoscale*, 2016, **8**, 4037–4046.
50 Z. Yan, L. Chen, M. Yoon and S. Kumar, *ACS Appl. Mater. Interfaces*, 2016, **8**, 33299–33306.
51 M. C. Barry, Z. Yan, M. Yoon, S. R. Kalidindi and S. Kumar, *Appl. Phys. Lett.*, 2018, **113**, 131902.
52 X. Yang, Z. Dai, Y. Zhao and S. Meng, *Phys. Chem. Chem. Phys.*, 2018, **20**, 15980–15985.
53 Z. G. Fthenakis and D. Tománek, *Phys. Rev. B: Condens. Matter Mater. Phys.*, 2012, **86**, 125418.

